Cortical tension regulates Hippo signaling via Par-1-mediated Kibra degradation

Sherzod A. Tokamov[1,2], Stephan Buiter[1], Anne Ullyot[1], Gordana Scepanovic[3], Audrey Miller Williams[1], Rodrigo Fernandez-Gonzalez[4], Sally Horne-Badovinac[1, 2], Richard G. Fehon[1, 2, *]

[1]Department of Molecular Genetics and Cell Biology, The University of Chicago, Chicago, IL 60637, USA.

[2]Committee on Development, Regeneration, and Stem Cell Biology, The University of Chicago, Chicago, IL 60637, USA.

[3]Department of Cell and Systems Biology, University of Toronto, Toronto, ON M5G 1M1, Canada.

[4]Institute of Biomedical Engineering and Department of Cell and Systems Biology, University of Toronto, Toronto, ON M5G 1M1, Canada.

[*]Correspondence and lead contact: rfehon@uchicago.edu

Abstract

The Hippo pathway is an evolutionarily conserved regulator of tissue growth. Multiple Hippo signaling components are regulated via proteolytic degradation. However, how these degradation mechanisms are themselves modulated remains unexplored. Kibra is a key upstream pathway activator that promotes its own ubiquitin-mediated degradation upon assembling a Hippo signaling complex. Here, we demonstrate that Hippo complex-dependent Kibra degradation is modulated by cortical tension. Using classical genetic, osmotic, and pharmacological manipulations of myosin activity and cortical tension, we show that increasing cortical tension leads to Kibra degradation, whereas decreasing cortical tension increases Kibra abundance. Our study also implicates Par-1 in regulating Kib abundance downstream of cortical tension. We demonstrate that Par-1 promotes ubiquitin-mediated Kib degradation in a Hippo complex-dependent manner and is required for tension-induced Kib degradation. Collectively, our results reveal a previously unknown molecular mechanism by which cortical tension affects Hippo signaling and provide novel insights into the role of mechanical forces in growth control.

Introduction

Elucidating the mechanisms that ensure robustness and reproducibility of organ size is a fundamental problem in cell and developmental biology. A key regulator of tissue growth in animals is the Hippo pathway. At its core, the Hippo pathway consists of a kinase cascade, composed of Ser/Thr kinases Hippo (Hpo) and Warts (Wts) and scaffold proteins Salvador (Sav) and Mats, that inhibits nuclear translocation of a pro-growth transcriptional co-activator, Yorkie (Yki). The activity of the kinase cascade is regulated by multiple upstream components, including a multivalent scaffold protein, Kibra (Kib). Kib localizes at the apical cell cortex of epithelial cells, where together with its binding partner, Merlin (Mer), it plays a key role in assembling and activating the Hippo kinase cascade to repress Yki activity. In the absence of a conventional receptor/ligand pair, however, little is known about how Kib activity is regulated.

A conserved feature of the Hippo pathway is its regulation via forces generated by F-actin and non-muscle myosin II (actomyosin). Actomyosin forces are regulated by the small GTPase RhoA (Rho1 in Drosophila), which can be activated or deactivated by guanine exchange factors (GEFs) or GTPase activating proteins (GAPs), respectively (Piekny et al., 2005). Rho1 potently stimulates actomyosin contractility by simultaneously activating Diaphanous, a formin that promotes linear F-actin bundle assembly, and Rho kinase (Rok), which phosphorylates and activates the myosin regulatory light chain (Lecuit et al., 2011). Studies over the years have shown that both F-actin polymerization and myosin activation stimulate the activity of Yki and its mammalian homologs, YAP/TAZ (Sansores-Garcia et al., 2011; Fernandez et al., 2011; Dupont et al., 2011; Wada et al., 2011; Aragona et al., 2013; Rauskolb et al., 2014; Ibar et al., 2018). Mechanistically, cytoskeletal tension was shown to promote Yki/YAP activity via LIM domain Ajuba family proteins, such as Ajuba (Jub), which accumulate at cell-cell junctions in response to tension and sequester Wts (Rauskolb et al., 2014; Pan et al., 2016; Ibar et al., 2018). However, this mechanism acts directly on the core kinase cascade, and it remains unclear whether or how tension could regulate the upstream Hippo signaling components, such as Kib.

A key determinant of signaling ouput downstream of Kib is its protein level. Loss of Kib results in tissue overgrowth via Yki activation, while the opposite occurs under ectopic Kib expression (Yu et al., 2010a; Genevet et al., 2010; Baumgartner et al., 2010; Su et al., 2017; Tokamov et al., 2021). Furthermore, upstream regulators, including Mer, Expanded and Kib, are transcriptionally upregulated by Yki, making their abundance a key component of a conserved negative feedback loop (Hamaratoglu et al., 2006; Genevet et al., 2010; Yee et al., 2019). Thus, control of Kib abundance provides an important point for modulating Kib-mediated Hippo pathway activation. In addition to transcriptional regulation, Kib abundance is regulated via ubiquitin-mediated proteolytic turnover (Tokamov et al., 2021). Upon assembly of the Hippo complex, Kib is ubiquitinated via the SCF^{Slimb} E3 ubiquitin ligase and subsequently degraded. This mechanism simultaneously requires a consensus recognition motif in Kib that recruits SCF^{Slimb}, as well as the two N-terminal WW domains in Kib that mediate Hippo complex formation. Notably, Kib levels are elevated in cells with lower cortical tension, suggesting that actomyosin-generated forces could regulate Kib abundance (Tokamov et al., 2021). How Kib levels are modulated by mechanical forces and whether this mechanism involves additional mechanosensitive components remains unknown.

In this study, using genetic, osmotic, and pharmacological manipulations of myosin activity, we report that actomyosin-generated cortical tension modulates Kib abundance. We find that increasing myosin activity and cortical tension lowers Kib abundance, while acutely inhibiting myosin activity elevates Kib levels. Importantly, we find that tension-mediated Kib

degradation occurs independently of the previously identified Jub-Wts mechanism. Instead, our results suggest that the serine/threonine kinase Par-1 promotes Kib degradation in a tension dependent manner. Together, our findings provide evidence that tension regulates upstream Hippo signaling and advance our understanding of how mechanical forces can influence the activity of a signaling pathway.

Results

Cortical tension promotes Kib degradation

Previously, we showed that Kib's role in assembling the Hippo signaling complex promotes its own degradation, thereby forming a post-translational negative feedback loop (Tokamov et al., 2021). Additionally, our results suggested that this feedback mechanism is modulated by cortical tension because cell clones under compression display higher levels of Kib than their neighbors. To better understand how Kib abundance is regulated, we sought to genetically manipulate non-muscle myosin II (myosin) contractility as a means to affect cortical tension. To visualize Kib, we used Kib tagged with the green fluorescent protein (GFP) and expressed under the ubiquitin promoter (Ubi>Kib-GFP), a transgene that we previously showed to be an effective reporter of post-translational changes in Kib abundance (Tokamov et al., 2021). We first transiently ectopically expressed RhoGEF2 to activate Rho1 upstream of myosin in the posterior compartment of the wing imaginal disc using the *hh>Gal4* driver combined with ubiquitously expressed $Gal80^{ts}$ ($tub>Gal80^{ts}$). Strikingly, expression of RhoGEF2 for 24h resulted in a significant decrease in Kib levels (Fig. 1A-B). Using phospho-specific antibody against the phosphorylated myosin regulatory light chain (pMRLC, Zhang and Ward, 2011), we confirmed that myosin activity was upregulated under these conditions (Fig. S1A-A''). Additionally, consistent with the function of Kib in repressing Yki and the role of tension in promoting Yki transcriptional activity (Genevet et al., 2010; Yu et al., 2010b; Baumgartner et al., 2010; Rauskolb et al., 2014), we saw increased nuclear Yki accumulation upon RhoGEF2 expression (Fig. S1B-B''). In contrast, the abundance of Ubi>$Kib^{\Delta WW1}$-GFP, a variant of Kib that is insensitive to Hippo complex-mediated degradation (Tokamov et al., 2021), was not affected by RhoGEF2 expression (Fig. 1C-D). These results are consistent with our previous observation that the abundance of wild-type Kib, but not $Kib^{\Delta WW1}$, was elevated in mosaic clones with decreased cortical tension (Tokamov et al., 2021) and suggest that cortical tension regulates Kib abundance via complex-mediated degradation.

We also previously showed that cortically localized Yki promotes myosin activation via a myosin light chain kinase called Stretchin (Strn-MLCK, Xu et al., 2018). Specifically, ectopic expression of myristoylated Yki (myr-Yki) leads to a significant increase in myosin activation. Therefore, we asked if myr-Yki expression also affected Kib levels. As with RhoGEF2 expression, ectopic myr-Yki expression substantially diminished Kib levels (Fig. 1E & F). Depletion of Strn-MLCK strongly suppressed the effect of myr-Yki, suggesting that this effect was mediated via myosin activity (Fig. 1E', F). However, Strn-MLCK depletion alone did not increase Kib levels (Fig. 1E'', F), so the physiological significance of this effect is unclear.

Changes in osmotic conditions alter myosin activity and cortical tension

Our genetic manipulations of cortical tension support the model that tension promotes Kib turnover. We sought to further test this model by acutely manipulating myosin activity and

103 cortical tension. Changes in osmotic pressure have been used extensively to alter cortical
104 cytoskeletal organization and tension (Di Ciano et al., 2002; Guilak et al., 2002; Sinha et al.,
105 2011; Boulant et al., 2011; Stewart et al., 2011; Pietuch et al., 2013; Diz-Muñoz et al., 2016;
106 Roffay et al., 2021). Therefore, we decided to subject wing imaginal discs to different osmotic
107 conditions (see Methods) and examine the effect on myosin activity and cortical tension. We
108 aimed to alter osmolarity gently enough to avoid cell death or tissue rupture and ensure
109 reversibility of the effected changes.
110 We first examined the effect of different osmotic conditions on myosin activity using the
111 anti-pMRLC antibody. Compared to isotonic controls, we saw a slight decrease in pMRLC
112 staining under hypertonic conditions, although this effect was not statistically significant, likely
113 due to the background associated with the antibody (Fig. 2A-B', D). Under hypotonic conditions,
114 however, we observed a substantial increase in pMRLC (Fig. 2C-D), indicating that osmotic
115 manipulations can acutely alter myosin activation. To ask if the observed changes in myosin
116 activity affected cortical tension, we performed laser-cutting experiments on individual bicellular
117 junctions and measured their initial recoil velocity. Because of the inherent heterogeneity of cell
118 junctional lengths and apical areas across the wing imaginal epithelium, we restricted all laser
119 cuts to the ventral-anterior region of the presumptive wing blade, which normally contains cells
120 with larger apical areas and longer junctions. Additionally, we were careful to avoid proximity to
121 mitotic cells (Fig. S2A). Consistent with the observed differences in pMRLC staining, we saw a
122 significant decrease in recoil velocities under hypertonic conditions and an even more significant
123 increase in recoil upon hypotonic shift (Fig. 2E-F, Movie 1). We observed no correlation between
124 junctional length and recoil velocities (Fig. S2B). Collectively, these results show that osmotic
125 manipulations can be used to acutely modulate myosin activity and cortical tension in the
126 imaginal epithelium.
127 To further validate that osmotically-altered cortical tension can induce biologically
128 relevant consequences, we once again examined the localization of Yki-YFP. Because tension is
129 known to promote nuclear Yki accumulation, we hypothesized that hypertonic conditions (lower
130 tension) should lead to less nuclear Yki, while hypotonic conditions should result in more
131 nuclear Yki. For these experiments, in order to see a definitive effect on Yki localization, we
132 increased the incubation time to 30 min. Consistent with our hypothesis, shifting tissues from an
133 isotonic to a hypertonic solution resulted in a decrease in nuclear Yki (Fig. S3A-B'', D).
134 Conversely, shifting to a hypotonic solution led to a dramatic increase in nuclear Yki (Fig. S3C-
135 D). To further demonstrate the significance of this effect, we decided to first concentrate Yki in
136 the nuclei under hypotonic conditions and then shift to a hypertonic environment. Hypotonically-
137 induced nuclear Yki accumulation was completely reversed after incubation in a hypertonic
138 solution (Fig. S3E-H). Together, these results show that osmotic manipulations can be used to
139 acutely modulate myosin activity and cortical tension in an epithelial monolayer with
140 biologically relevant consequences.

141 **Osmotic shifts affect Kib abundance**

142 Given our result that changes in the medium osmolarity can influence cortical tension, we asked
143 if the osmotic manipulations also affected Kib abundance. Compared to isotonic conditions,
144 incubating tissues in a hypertonic solution resulted in an increased Kib abundance at the apical
145 cortex (Fig. 3A, B, & D). Moreover, Kib fluorescence also increased in more basal tissue
146 sections, suggesting that the apical increase in Kib was not due to apical recruitment from the
147 cytoplasmic pool (Fig. 3E). Conversely, in tissues incubated in a hypotonic solution, Kib

148 abundance decreased dramatically both at the apical cortex and in more basal tissue sections
149 compared to isotonic controls (Fig. 3C-E). In contrast, fluorescence intensity of Ubi>Kib$^{\Delta WW1}$-
150 GFP did not change significantly under osmotic shifts (Fig.S4A-C), suggesting that osmotically-
151 induced Kib degradation is mediated via the previously described Hippo complex-dependent
152 mechanism (Tokamov et al., 2021). These results demonstrate that cortical tension can rapidly
153 modulate Kib abundance.
154 We also considered the possibility that changes in apical area could alter Kib distribution
155 and fluorescence intensity by concentrating or diluting the protein at the cortex. To address this
156 point, we first measured fluorescent intensity of a junctional marker, Ecad-mKate2, and saw no
157 significant changes under osmotic shifts (Fig. 3F). Next, we measured apical cell areas upon
158 shifting wing imaginal tissues from isotonic to hypotonic or hypertonic conditions. Immediately
159 after the addition of the hypotonic solution, apical areas increased rapidly during the first ~3 min
160 of incubation (Fig. 3G). However, this initial increase was followed by a steady decrease of areas
161 in the next 12 min, until on average the areas returned roughly to their initial values (Fig. 3G,
162 Movie 2). Similarly, addition of the hypertonic solution resulted in a transient reduction in apical
163 areas during the first ~3 min, followed by a steady return to their starting values by 15 min of
164 incubation (Fig. 3H, Movie 3). Because we measured Kib fluorescence after 15 min of
165 incubation (Fig. 3A-C), changes in apical area are unlikely to explain the observed changes in
166 cortical Kib abundance under osmotic shifts. Collectively, these results suggest that changes in
167 myosin activity may be responsible for changes in Kib abundance under osmotic shifts.

168 **Inhibition of myosin activity blocks Kib degradation under hypotonic conditions**
169 If myosin-generated cortical tension is responsible for the observed decrease in Kib abundance
170 under hypotonic shift, then inhibiting myosin activity under these conditions should block Kib
171 degradation. To test this idea, we used Y-27632, a pharmacological inhibitor of Rho kinase (Rok)
172 activity (Uehata et al., 1997). Under isotonic conditions, we observed a slight reduction in
173 pMRLC staining when tissues were treated with Y-27632 (Fig. 4A-B'), though this effect was
174 not statistically significant (Fig. 4I; again, possibly obscured by high antibody background
175 staining). However, Y-27632 potently inhibited myosin hyperactivation induced by hypotonic
176 conditions (Fig. 4C-D', I).
177 We next asked if Y-27632 treatment would affect Kib abundance. Strikingly, we observed
178 a substantial increase in Kib abundance after 15 min of Y-27632 treatment under isotonic
179 conditions (Fig. 4E, F, & J), supporting the idea that myosin activity promotes Kib degradation.
180 To test if Rok inhibition could block the effect of hypotonic conditions, we incubated tissues in a
181 hypotonic solution containing Y-27632. Addition of Y-27632 strongly blocked the effect of the
182 hypotonic medium on Kib abundance (Fig. 4G, H, & J), suggesting that the effect of osmotic
183 shifts on Kib abundance is caused by myosin activity.
184 We also considered the possibility that the effect of Y-27632 could be mediated via
185 inhibition of another known target of this inhibitor, the atypical protein kinase C (aPKC). To test
186 this possibility, we took advantage of a conditional allele of aPKC, *aPKC^{as4}* that can be acutely
187 inhibited using 1NA-PP1, an allele-specific analog of a potent kinase inhibitor (Hannaford et al.,
188 2019a). As expected, under normal conditions, aPKC^{as4} was enriched at the apical cortex in the
189 wing imaginal epithelium (Fig. S5A-A'). In contrast, treatment with 1NA-PP1 severely inhibited
190 aPKC cortical localization (Fig. S5B-B'). On the other hand, treatment with Y-27632 did not
191 significantly affect aPKC cortical localization in wild type imaginal discs (Fig. S5C-D').
192 Additionally, we treated wing discs homozygous for *aPKC^{as4}* allele with 1NA-PP1 and did not

observe any changes in Kib abundance upon aPKC inhibition (Fig. S5E-G). These results show that the effect of Y-27632 on Kib abundance is not due to aPKC inhibition and instead suggest that Kib degradation under hypotonic conditions is mediated via cortical tension.

Par-1 regulates Kib abundance

How can tension influence abundance of a signaling protein such as Kib? Previous work identified a mechanism whereby tension inhibits Hippo signaling via Jub-mediated sequestration and inactivation of Wts/LATS at the cell-cell junctions (Rauskolb et al., 2014; Ibar et al., 2018). Surprisingly, although we observed a significant increase in myosin activity under hypotonic conditions (Fig. 2C), we did not detect significant changes in cortical Jub (Fig. S6A-D). Additionally, loss of Jub does not affect Kib levels (Fig. S6E). These observations suggest that cortical tension regulates Kib abundance independently of Jub.

Recently, cortical tension was shown to promote cortical localization of Par-1 in the Drosophila oocyte (Doerflinger et al., 2021). Interestingly, Par-1 mediates proteolytic degradation of an $SCF^{Slimb/\beta TrCP}$ substrate Oskar (Morais-de-Sá et al., 2013) and is known to physically associate with Hippo signaling components and regulate tissue growth (Huang et al., 2013, p. 1). We therefore hypothesized that cortical tension could promote Kib degradation via Par-1. To test this idea, we first asked if Par-1 regulates Kib abundance using Ubi>Kib-GFP as a reporter. Kib levels increased significantly upon Par-1 depletion (Figs. 5A & C, S7A), whereas ectopic Par-1 expression resulted in a significant reduction in Kib levels (Fig. 5B & C). In contrast, loss of Par-1 did not affect the abundance of $Kib^{\Delta WW1}$ (Fig. 5D & E), suggesting that Par-1 regulates Kib levels via Kib-mediated Hippo complex assembly (Tokamov et al., 2021).

Par-1 was previously shown to promote Hpo phosphorylation on Ser30, which inhibits Hpo activity (Huang et al., 2013). Therefore, we considered the possibility that the increase in Kib abundance under loss of Par-1 was indirectly caused by the lack of Hpo phosphorylation on Ser30. If this were the case, we reasoned that ectopic expression of Hpo construct that is refractory to Par-1 phosphorylation (Hpo^{S30A}), would also lead to increased Kib abundance. To this end, we first transiently expressed wild-type Hpo in the posterior compartment of the wing imaginal disc and examined the effect on Kib levels. Consistent with our previous finding that Hpo promotes Kib ubiquitination and degradation (Tokamov et al., 2021), Kib levels decreased significantly under ectopic Hpo expression (Fig. S7B). Importantly, ectopic expression of Hpo^{S30A} also induced a decrease in Kib abundance (Fig. S7C), suggesting that the effect of Par-1 on Kib abundance is not mediated through Hpo phosphorylation.

We have previously shown that Kib is ubiquitinated via $SCF^{Slimb/\beta TrCP}$ in cultured Schneider's 2 (S2) cells. Because Par-1 is a kinase and is known to function with $SCF^{Slimb/\beta TrCP}$, we asked if Par-1 affects Kib ubiquitination or phosphorylation in S2 cells. We observed that while Kib was ubiquitinated in control cells, Par-1 depletion led to a strong decrease in Kib ubiquitination (Fig. 5F). To test if Par-1 promotes Kib phosphorylation, we performed gel-shift assays in the presence of wild type or kinase-dead Par-1 ($Par\text{-}1^{KD}$). Kib is normally phosphorylated in S2 cells, as it appears as a smeary, slow migrating band that collapses into a single, faster migrating band with phosphatase treatment (Fig. 5G, Tokamov et al., 2021). Addition of active Par-1, but not $Par\text{-}1^{KD}$, resulted in an upward shift of Kib band and disappearance of the lower, non-phosphorylated pool, suggesting that Par-1 promotes Kib phosphorylation (Fig. 5G). Together, these results suggest that Par-1 regulates ubiquitin-mediated Kib degradation, possibly in a phosphorylation-dependent manner, and that tension could modulate Kib abundance via Par-1.

238 **Cortical tension promotes Par-1 association with the cortex**
239 Given the previous report that myosin activity promotes cortical Par-1 localization in the
240 *Drosophila* oocyte (Doerflinger et al., 2021), we wondered if a similar effect could be observed
241 in the wing imaginal epithelium. To this end, we first examined Par-1 localization in control cells
242 or in cells overexpressing RhoGEF2. Although known as a basolateral component, in the
243 Drosophila blastoderm Par-1 also localizes at the apicolateral cortex (Bayraktar et al., 2006). In
244 the wing imaginal disc, Par-1 displayed apical and basolateral localization, though its
245 localization appeared diffuse in both places (Fig. 6A & A'). Transient overexpression of
246 RhoGEF2 resulted in sharper Par-1 localization at the cell cortex both apically and basolaterally
247 (Fig. 6B & B'), suggesting that tension can affect Par-1 cortical association. As an alternative
248 approach, we also examined Par-1 localization using Airyscan confocal microscopy under
249 hypotonic conditions. Similar to ectopic RhoGEF2 expression, Par-1 was more tightly associated
250 with the apical and basolateral cortex under hypotonic compared to isotonic conditions (Fig. 6C-
251 D'). These results suggest that tension promotes Par-1 association with the cell cortex.

252 **Par-1 is required for tension-dependent degradation of Kib**
253 We reasoned that if tension regulates in Kib abundance via Par-1, then in the absence of Par-1
254 tension would have no effect on Kib levels. To test this idea, we depleted Par-1 in the posterior
255 compartment of the wing imaginal disc using the *hh>Gal4* driver and quantified changes in Kib
256 levels when tissues were shifted from isotonic to hypotonic conditions. While we observed a
257 significant decrease in Kib intensity in the anterior (control) compartment, there was no
258 significant change in the posterior (Par-1 depleted) compartment (Fig. 6E-G). Collectively, these
259 results are consistent with the idea that tension modulates Kib abundance by controlling Par-1
260 cortical association.

261 **Discussion**
262 Elucidating the molecular mechanisms that control the abundance of individual signaling
263 components has been central to our understanding how the Hippo pathway is regulated (Ribeiro
264 et al., 2014; Bosch et al., 2014; Rodrigues-Campos and Thompson, 2014; Aerne et al., 2015; Ma
265 et al., 2018; Fulford et al., 2019; Wang et al., 2019; Misra and Irvine, 2019; Tokamov et al.,
266 2021). However, how these different mechanisms themselves are regulated has been a poorly
267 understood and intriguing area of investigation. Our work reveals a previously unrecognized role
268 of cortical tension in modulating the abundance of a key upstream Hippo pathway component,
269 Kib. Using a combination of genetic, osmotic, and pharmacological approaches, we demonstrate
270 that cortical tension promotes Kib degradation. Our study also implicates Par-1 in mediating Kib
271 degradation downstream of cortical tension. This work advances our understanding of how
272 tension regulates Hippo signaling and provides novel insights into the role of mechanical forces
273 in tissue growth and patterning.
274 We provide several lines of evidence that Kib is degraded as a result of myosin-generated
275 tension. First, we show that activation of myosin via two different myosin light chain kinases,
276 Rok (in the case of ectopic RhoGEF2 expression and Y-27632 treatment) and Strn-MLCK (in the
277 case of ectopic myr-Yki expression) decreases Kib abundance (Figs. 1 & 4), suggesting that Kib
278 degradation occurs irrespective of the upstream mechanisms of myosin activation. Second,
279 although RhoGEF2 is known to promote both myosin activity and formin-mediated F-actin
280 assembly, we did not observe a detectible effect on F-actin under transient RhoGEF2 expression,

281 whereas myosin activity was substantially upregulated (Fig. S1). Third, we develop a simple,
282 non-genetic and acute approach to dramatically increase myosin activity using hypotonic
283 conditions and demonstrate that myosin activation using this method results in Kib degradation
284 (Figs. 2-4). Thus, we propose that Kib degradation is modulated by cortical tension downstream
285 of myosin activity.
286 Our results also suggest that Kib degradation downstream of cortical tension is mediated
287 via Hippo complex formation. We have shown previously that Kib targets itself for ubiquitin-
288 mediated degradation upon Hippo complex assembly, and this process requires Kib's WW1
289 domain and a consensus degron motif recognized by $SCF^{Slimb/\beta TrCP}$ (Tokamov et al., 2021). In this
290 study, we observe that the abundance of wild-type Kib, but not $Kib^{\Delta WW1}$, is modulated via
291 myosin activity, raising the question of how tension can promote complex-dependent Kib
292 turnover. In the simplest scenario, cortical tension could promote the association of existing Kib
293 complexes with a tension-sensitive component capable of modulating Kib levels. We identify
294 Par-1 as a potential link in this process. Cortical tension was previously reported to promote
295 cortical Par-1 localization in the *Drosophila* oocyte (Doerflinger et al., 2021). Here, we show that
296 Par-1 promotes turnover of wild-type Kib, but not $Kib^{\Delta WW1}$, in vivo and regulates Kib
297 phosphorylation and ubiquitination in cultured cells (Fig. 5). Importantly, cortical tension fails to
298 induce Kib turnover in cells depleted of Par-1 (Fig. 6). Based on these results, and our
299 observations that Par-1 becomes more tightly associated with the cell cortex under increased
300 cortical tension (Fig. 6), we propose that cortical tension could regulate Kib levels at least in part
301 by modulating the association of Par-1 with Kib signaling complexes. Interestingly, a recent
302 study in human cells also suggested that tension generated at the ECM promotes degradation of a
303 Hpo homolog, MST2, by modulating the physical interaction between MST2 and $SCF^{Slimb/\beta TrCP}$
304 complex (Fiore et al., 2022). Thus, in a more complex scenario, cortical tension could also
305 regulate Kib association with multiple components of the degradation machinery, including
306 $SCF^{Slimb/\beta TrCP}$.
307 This study also highlights the recurring role of Par-1 in the regulation of Hippo signaling.
308 Previous work suggested that Par-1 phosphorylates Hpo, which prevents Hpo association with
309 Sav (Huang et al., 2013). Here, we find that Par-1 regulates Kib abundance independently of Hpo
310 phosphorylation. Our observation that Par-1 regulates the abundance of wild-type Kib but not
311 $Kib^{\Delta WW1}$ suggests that Par-1 regulates Kib via the Hippo complex-mediated degradation
312 mechanism involving $SCF^{Slimb/\beta TrCP}$ (Tokamov et al., 2021). This idea is supported by a previous
313 report that Par-1 functions with $SCF^{Slimb/\beta TrCP}$ in promoting turnover of Oscar during Drosophila
314 oocyte development (Morais-de-Sá et al., 2013). Notably, active Par-1 was also found to be a
315 target of $SCF^{Slimb/\beta TrCP}$-mediated degradation (Lee et al., 2012), further highlighting the tight
316 association between Par-1, $SCF^{Slimb/\beta TrCP}$, and Kib. It is still unclear what happens to the rest of
317 the Hippo signaling complex after Kib is degraded, but the multifaceted function of Par-1 in
318 inhibiting Hpo activity, Hpo-Sav interaction, and promoting Kib degradation could provide the
319 means of dissociating the entire signaling complex upon Kib turnover.
320 One of the surprising observations in our study is that while cortical tension induced by
321 hypotonic conditions triggers Kib degradation, it does not affect junctional Jub accumulation.
322 Previous work has shown that increasing myosin activity via genetic manipulations enhances Jub
323 recruitment to the adherens junctions, where Jub sequesters Wts (Rauskolb et al., 2014). This
324 recruitment is thought to be mediated via tension-induced opening of α-catenin conformation,
325 which exposes a region in α-catenin that binds Jub (Rauskolb et al., 2014; Alégot et al., 2019;
326 Sarpal et al., 2019). Combined with these reports, our observations suggest that hypotonically-

327 induced myosin activation may differ from that achieved via common genetic manipulations.
328 Most obviously, this difference could be temporal – hypotonic treatment of wing imaginal discs
329 induces dramatic myosin activation and Kib degradation within 15 minutes (Fig. 2), whereas
330 genetic manipulations are done in the order of hours or days. Thus, α-catenin-mediated
331 recruitment of Jub could occur at a longer timescale compared to the more dynamic Kib
332 turnover. Counter to this argument, a recent study observed rapid junctional accumulation of Jub-
333 Wts clusters at sites of high tension in the Drosophila developing notum (López-Gay et al.,
334 2020). An alternative explanation is that hypotonically-induced myosin activation does not result
335 in α-catenin conformational changes. The opening of α-catenin conformation at bicellular
336 junctions is thought to be triggered via actomyosin forces applied orthogonally to the junctions
337 (Rauskolb et al., 2019; López-Gay et al., 2020). This is unlikely to be the case under hypotonic
338 conditions, where actomyosin generated forces would be generated parallel to the lateral
339 membrane to counteract the mechanical stretching induced by hydrostatic pressure.
340 Finally, our study raises the question of the biological importance of tension-dependent
341 Kib degradation. In the growing wing imaginal epithelium, cortical tension was shown to be
342 higher at the tissue periphery than at the tissue center (LeGoff et al., 2013; Mao et al., 2013).
343 Greater tension at the periphery was proposed to drive growth, possibly via Yki activity, to
344 compensate for the lower concentration of growth-stimulating morphogens, which diffuse from
345 narrow stripes of cells at the center of the tissue (Aegerter-Wilmsen et al., 2007, 2012;
346 Hariharan, 2015; Pan et al., 2016). Additionally, we have previously reported that Kib
347 degradation occurs more prominently at the tissue periphery, where cortical tension is higher
348 (Tokamov et al., 2021). Based on these studies, we propose that tension-mediated Kib
349 degradation could serve to pattern Hippo signaling activity, and therefore growth, across a
350 growing epithelium such as the wing imaginal disc. How Kib degradation and other tension-
351 regulated mechanisms, such as the Jub-Wts mechanism, are coordinated to control the Hippo
352 pathway and growth remains unanswered. However, we believe this study provides valuable
353 insights for future investigation of the molecular mechanisms by which mechanical forces affect
354 tissue growth.

355 **Methods**

356 **Table 1: Reagents**

Reagent type (species) or resource	Designation	Source or reference	Identifiers	Additional information
genetic reagent (*D. melanogaster*)	*Ubi>Kib-GFP-FLAG*	(Tokamov et al., 2021)		
genetic reagent (*D. melanogaster*)	*Ubi-Kib$^{\Delta WW1}$-GFP-FLAG*	(Tokamov et al., 2021)		
genetic reagent (*D. melanogaster*)	*UASp-T7-RhoGEF2*	Bloomington Drosophila Stock Center	BL9387	
genetic reagent (*D. melanogaster*)	*UASt-myr-Yki*	10.1016/j.devcel.2018.06.017		
genetic reagent (*D. melanogaster*)	*UAS-Strn RNAi*	Bloomington Drosophila Stock Center	BL26736	Validated in 10.1016/j.devcel.2018.06.017
genetic reagent (*D. melanogaster*)	*UAS-Par-1 RNAi*	Bloomington Drosophila Stock Center	BL32410	
genetic reagent (*D. melanogaster*)	*UAS-jub RNAi*	Bloomington Drosophila Stock Center	BL30806	Validated in 10.1016/j.cub.2010.02.035
genetic reagent (*D. melanogaster*)	*Ecad-3XmKate2*	(Pinheiro et al., 2017)		

genetic reagent (*D. melanogaster*)	*Par-1:GFP (protein trap)*	Bloomington Drosophila Stock Center	BL64452	
genetic reagent (*D. melanogaster*)	*Jub:GFP*	Bloomington Drosophila Stock Center	BL56806	
genetic reagent (*D. melanogaster*)	w^{1118}; yki^{B5} {*yki-YFP*} *VK37*	(Xu et al., 2018)		
genetic reagent (*D. melanogaster*)	$aPKC^{as4}$	(Hannaford et al., 2019b)		
Antibody	anti-pSqh (Guinea pig, polyclonal)	(Zhang and Ward, 2011)		Tissue staining (1:300)
Antibody	anti-DEcad (Rat, polyclonal)	Developmental Studies Hybridoma Bank	Cat#AB_528120; RRID:AB_528120	Tissue staining (1:1000)
Antibody	anti-PKC, rabbit polyclonal	Santa Cruz Biotechnology	Lot#: G2304	tissue staining (1:1000)
Antibody	anti-GFP, guinea pig, polyclonal	(Yee et al., 2019)		IP (1:1250)
Antibody	anti-GFP, rabbit, polyclonal	Michael Glotzer, (University of Chicago)		IB (1:5000)
Chemical	Y-27632	Fisher Scientific	Cat. # 12541	Rho kinase inhibitor

Chemical	1-NA-PP1	Cayman	Cat. # CAYM-10954-1	ATP analog

357 ***Drosophila* husbandry**
358 *Drosophila melanogaster* was cultured using standard techniques at 25°C (unless otherwise
359 noted). For Gal80^{ts} experiments, crosses were maintained at 18°C until larvae reached late
360 second or early third instar stages and shifted to 29°C for the duration specified in each
361 experiment. Immediately after incubation at 29°C, wing imaginal tissues were dissected from
362 wandering third instar larvae and imaged live.

363 **Live imaging**
364 Throughout the study (except in Figs. 2A-C', 4A-D', S1A-A', S5A-D'), wing imaginal discs
365 were imaged live. Imaging of live tissues was performed as previously described (Xu et al.,
366 2019). Briefly, freshly dissected wing imaginal discs from third instar larvae were pipetted into a
367 ~40 ml droplet of Schneider's Drosophila Medium supplemented with 10% fetal bovine serum
368 and mounted on a glass slide. To support the tissue, spherical glass beads (Cospheric, Product
369 ID: SLGMS-2.5) of ~50 mm in diameter were placed under the cover slip. The mounted samples
370 were immediately imaged.
371 For osmotic shifts, Y-27632 treatment, and laser ablation experiments, live imaging
372 method was adapted from Restrepo et al. (2016). Briefly, wing imaginal tissues were first
373 dissected in Schneider's Drosophila Medium (Sigma) supplemented with 10% Fetal Bovine
374 Serum (Thermo Fisher Scientific). The tissues were then transferred with a pipette in 5-10µl of
375 medium to a glass bottom microwell dish (MatTek, 35mm petri dish, 14mm microwell) with No.
376 1.5 coverglass. The discs were oriented so that the apical side of the disc proper faced the
377 coverglass. A Millicell culture insert (Sigma, 12mm diameter, 8µm membrane pore size) was
378 prepared in advance by cutting off the bottom legs with a razor blade and removing any excess
379 membrane material around the rim of the insert. The insert was carefully placed into the 14mm
380 microwell space, directly on top of the drop containing properly oriented tissues. To prevent the
381 tissue from moving, the space between the insert and the microwell was sealed with ~10µl of
382 mineral oil. Media with indicated osmolarity and/or chemical inhibitor was then added into the
383 chamber of the insert (200µl in all experiments). An inverted Zeiss LSM880 laser scanning
384 confocal microscope equipped with a GaAsP spectral detector and the Airyscan module was used
385 for all imaging (except for laser ablation experiments, see below).

386 **Osmotic shift experiments**
387 Schneider's Drosophila Medium (Sigma) supplemented with 10% Fetal Bovine Serum (Thermo
388 Fisher Scientific) was used as isotonic medium (~360mOsm). To make a hypertonic solution, the
389 osmolarity of the isotonic solution was increased to ~460mOsm using 1M NaCl. To make a
390 hypotonic solution, the isotonic medium was diluted with deionized water to ~216mOsm. All
391 osmotic solutions were prepared fresh immediately before the experiments. In most experiments,
392 tissues were incubated for 15 min in a humid chamber before mounting (see above). For practical
393 reasons, in laser ablation experiments tissues were incubated for 8 min to allow for
394 measurements to be taken at an average of 15 min under osmotic incubations.

395 To observe changes in Yki-YFP localization, flies expressing BAC recombineered Yki-
396 YFP in the background of *yki*^{B5} null allele were used. Ubi>RFP^{nls} was also expressed in the
397 background to mark the nuclei. Tissues were dissected and mounted as described above. Each
398 wing disc was first imaged under isotonic conditions, with 4-5 optical sections taken in the basal
399 plane where the nuclei were clearly identifiable. The isotonic medium was then replaced with an
400 indicated osmotic solution, and after 30 min of incubation, each tissue was reacquired in the
401 same order and roughly the same optical plane. The steps were repeated for the third osmotic
402 condition.

403 **pMRLC staining experiments**
404 Wandering third instar larvae were dissected in an isotonic solution and the wing imaginal discs
405 were transferred into a 150µl drop of freshly prepared osmotic medium. For experiments with Y-
406 27632, osmotic media with 50µM of Y-27632 were prepared. The tissues were incubated for 15
407 min. After incubation, the discs were washed with 1X Ringer's buffer with correspondingly
408 adjusted osmolarity (i.e. for hypertonic experiments, a hypertonic wash was prepared the same
409 way as described above, except 1X Ringer's was used instead of the Schneider's medium) and
410 fixed for 20 min in 2% paraformaldehyde/1X Ringer's solution also with properly adjusted
411 osmolarity (for Y-27632 experiments, 50µM of Y-27632 was also added in the wash and the fix
412 solutions). Tissues were then stained with the primary antibody against the *Drosophila* phospho-
413 MRLC (anti-pSqh, see Table 1) and secondary antibodies as previously described (McCartney
414 and Fehon, 1996).

415 **Laser ablation of bi-cellular junctions**
416 Laser cuts were conducted using a pulsed Micropoint nitrogen laser (Andor Technology) tuned to
417 365 nm and mounted on an Andor Revolution XD spinning disk confocal microscope. Individual
418 junctions were ablated by delivering 3 pulses at a single point with a duration of 67 ms/pulse.
419 Each tissue was imaged 2x before and 20x immediately after ablation, with a time interval of 4 s.
420 Images were acquired using a 100X oil-immersion lens (Olympus, NA 1.40), an iXon Ultra 897
421 camera (Andor), and Metamorph (Molecular Devices) as the image acquisition software.
422 Sixteen-bit Z-stacks were collected at each time point consisting of 7 slices with 0.5 µm interval.
423 To measure initial recoil velocity, the positions of the two tricellular vertices connected
424 by the ablated junction were manually tracked using the SIESTA image analysis platform
425 (Fernandez-Gonzalez and Zallen, 2011), and the initial retraction velocities were calculated using
426 custom MATLAB scripts.

427 **Image analysis, quantification of fluorescence intensities and apical areas**
428 All images were processed in ImageJ. For apical Kib-GFP, Kib$^{\Delta WW1}$-GFP, Jub-GFP, and Ecad-
429 mKate2 mean fluorescence intensity measurements were taken from maximum intensity
430 projections (~0.75 µm/section, four to six sections from apical surface). For basal Kib-GFP mean
431 fluorescence intensity measurements, single basal optical sections were used (~7.5-10µm below
432 the apical surface). To quantify changes in pMRLC intensity, mean fluorescence measurements
433 were obtained from single most apical sections. Plots and statistical analyses of mean
434 fluorescence intensities were generated using GraphPad Prism software.
435 To measure changes in apical cell areas under osmotic shifts, cells from Ecad-GFP
436 labeled epithelia were segmented using the Cellpose v1 pre-trained "cytoplasm" model
437 (Stringer et al., 2021) and tracked via a previously-described tracking algorithm (Williams

438 et al., 2022). Errors in segmentation and tracking were corrected manually. Only cells that
439 remained in the field of view for the entire timelapse duration were used for quantification.
440 The mean and standard error in cell areas were measured per epithelium. Fold-change in
441 area relative to the start of osmotic shift was plotted using the Matplotlib library in Python.
442 To quantify nuclear/cytoplasmic Yki-YFP, single optical sections were used. Ubi>RFP
443 channel was used to segment the nuclei using Cellpose and a standard Scikit watershed algorithm
444 (van der Walt et al., 2014) to generate a nuclear mask. The nuclear mask was then applied to Yki-
445 YFP images to extract nuclear Yki-YFP intensities, and the signal outside the nuclear mask was
446 treated as cytoplasmic. The ratios of nuclear to cytoplasmic intensity was then calculated and
447 plotted.

448 **Detection of Kibra ubiquitination in S2 cells**

449 Kib ubiquitination assay was performed as described previously (Tokamov et al., 2021). Briefly,
450 3.5 x 10^6 S2 cells (S2-DGRC) were transfected with a total of 500 ng of indicated DNA using
451 dimethyldioctadecylammonium bromide (Sigma; Han, 1996) at 250 mg/ml in six-well plates.
452 pMT-Kib-GFP was co-transfected with pMT-HA-Ub (Zhang et al., 2006) where indicated to
453 provide labeled ubiquitin. To induce expression of the pMT constructs, 700 mM CuSO4 was
454 added to the wells 24 hr prior to cell lysis (2 days after transfection). To inhibit proteasomal
455 degradation, 50 mM MG132 (Cayman Chemical) and 50 mM calpain inhibitor I (Sigma Aldrich)
456 was added 4 hr prior to cell lysis. Cells were lysed in RIPA buffer (150 mM NaCl, 1% NP-40,
457 0.5% Na deoxycholate, 0.1% SDS, and 25 mM Tris [50 mM, pH 7.4]), supplemented with 5 mM
458 N-ethylmaleimide and Complete protease inhibitor cocktail (Roche, one tablet/10 ml of buffer).
459 HA-tagged ubiquitin was purified using Pierce anti-HA magnetic beads (clone 2–2.2.14). Lysates
460 and IP samples were run on 8% polyacrylamide gel and ubiquitinated Kib in the IP samples was
461 detected by Western Blot using anti-GFP antibody (rabbit, see Table 1).

462 **Detection of Kibra phosphorylation in S2 cells**

463 pMT-Kib-GFP and pAHW-Par-1 or pAHW-Par-1^{KD} (gift from Bingwei Lu, Stanford University)
464 were transfected and expression was induced as described above. Immunoprecipitation (IP) was
465 performed 3 days after transfection. To induce expression of pMT-Kib-GFP, 700 mM CuSO4
466 was added to the wells 24 hr prior to cell lysis (2 days after transfection).
467 Cells were harvested and lysed on ice in buffer containing 25 mM Hepes, 150 mM NaCl, 1 mM
468 ethylenediaminetetraacetic acid, 0.5 mM ethylene glycol-bis(b-aminoethyl ether)-N,N,N0,N0-
469 tetraacetic acid, 0.9 M glycerol, 0.1% Triton X-100, 0.5 mM Dithiothreitol, and Complete
470 protease inhibitor (Roche) and PhosSTOP (Sigma Aldrich) phosphatase inhibitor cocktails at
471 one tablet/10 ml concentration each. Cell lysates were then incubated with anti-GFP antibody
472 (guinea pig, see Table 1) for 30min. Antibody-bound Kib-GFP was pulled down using Pierce
473 Protein A magnetic beads (Thermo Scientific) for 1.5h. A control immunoprecipiated sample was
474 treated with λ-phosphatase. Samples were run on 8% polyacrylamide gel, with 118:1
475 acrylamide/bisacrylamide (Scheid et al., 1999), to better resolve phosphorylated Kib species. Kib
476 was detected by Western Blot using anti-GFP antibody (rabbit, see Table 1).

References

Aegerter-Wilmsen, T., Aegerter, C.M., Hafen, E., Basler, K., 2007. Model for the regulation of size in the wing imaginal disc of Drosophila. Mechanisms of Development 124, 318–326. https://doi.org/10.1016/j.mod.2006.12.005

Aegerter-Wilmsen, T., Heimlicher, M.B., Smith, A.C., de Reuille, P.B., Smith, R.S., Aegerter, C.M., Basler, K., 2012. Integrating force-sensing and signaling pathways in a model for the regulation of wing imaginal disc size. Development 139, 3221–3231. https://doi.org/10.1242/dev.082800

Aerne, B.L., Gailite, I., Sims, D., Tapon, N., 2015. Hippo Stabilises Its Adaptor Salvador by Antagonising the HECT Ubiquitin Ligase Herc4. PLOS ONE 10, e0131113. https://doi.org/10.1371/journal.pone.0131113

Alégot, H., Markosian, C., Rauskolb, C., Yang, J., Kirichenko, E., Wang, Y.-C., Irvine, K.D., 2019. Recruitment of Jub by α-catenin promotes Yki activity and *Drosophila* wing growth. Journal of Cell Science 132, jcs222018. https://doi.org/10.1242/jcs.222018

Aragona, M., Panciera, T., Manfrin, A., Giulitti, S., Michielin, F., Elvassore, N., Dupont, S., Piccolo, S., 2013. A Mechanical Checkpoint Controls Multicellular Growth through YAP/TAZ Regulation by Actin-Processing Factors. Cell 154, 1047–1059. https://doi.org/10.1016/j.cell.2013.07.042

Baumgartner, R., Poernbacher, I., Buser, N., Hafen, E., Stocker, H., 2010. The WW Domain Protein Kibra Acts Upstream of Hippo in Drosophila. Developmental Cell 18, 309–316. https://doi.org/10.1016/j.devcel.2009.12.013

Bayraktar, J., Zygmunt, D., Carthew, R.W., 2006. Par-1 kinase establishes cell polarity and functions in Notch signaling in the *Drosophila* embryo. Journal of Cell Science 119, 711–721. https://doi.org/10.1242/jcs.02789

Bosch, J.A., Sumabat, T.M., Hafezi, Y., Pellock, B.J., Gandhi, K.D., Hariharan, I.K., 2014. The Drosophila F-box protein Fbxl7 binds to the protocadherin Fat and regulates Dachs localization and Hippo signaling. eLife 3, e03383. https://doi.org/10.7554/eLife.03383

Boulant, S., Kural, C., Zeeh, J.-C., Ubelmann, F., Kirchhausen, T., 2011. Actin dynamics counteract membrane tension during clathrin-mediated endocytosis. Nat Cell Biol 13, 1124–1131. https://doi.org/10.1038/ncb2307

Di Ciano, C., Nie, Z., Szászi, K., Lewis, A., Uruno, T., Zhan, X., Rotstein, O.D., Mak, A., Kapus, A., 2002. Osmotic stress-induced remodeling of the cortical cytoskeleton. American Journal of Physiology-Cell Physiology 283, C850–C865. https://doi.org/10.1152/ajpcell.00018.2002

Diz-Muñoz, A., Thurley, K., Chintamen, S., Altschuler, S.J., Wu, L.F., Fletcher, D.A., Weiner, O.D., 2016. Membrane Tension Acts Through PLD2 and mTORC2 to Limit Actin Network Assembly During Neutrophil Migration. PLoS Biol 14, e1002474. https://doi.org/10.1371/journal.pbio.1002474

Doerflinger, H., Zimyanin, V., St Johnston, D., 2021. The Drosophila anterior-posterior axis is polarized by asymmetric myosin activation. Current Biology S0960982221015487. https://doi.org/10.1016/j.cub.2021.11.024

Dupont, S., Morsut, L., Aragona, M., Enzo, E., Giulitti, S., Cordenonsi, M., Zanconato, F., Le Digabel, J., Forcato, M., Bicciato, S., Elvassore, N., Piccolo, S., 2011. Role of YAP/TAZ in mechanotransduction. Nature 474, 179–183. https://doi.org/10.1038/nature10137

521 Fernandez, B.G., Gaspar, P., Bras-Pereira, C., Jezowska, B., Rebelo, S.R., Janody, F., 2011.
522 Actin-Capping Protein and the Hippo pathway regulate F-actin and tissue growth in
523 Drosophila. Development 138, 2337–2346. https://doi.org/10.1242/dev.063545
524 Fiore, A.P.Z.P., Rodrigues, A.M., Ribeiro-Filho, H.V., Manucci, A.C., de Freitas Ribeiro, P.,
525 Botelho, M.C.S., Vogel, C., Lopes-de-Oliveira, P.S., Pagano, M., Bruni-Cardoso, A.,
526 2022. Extracellular matrix stiffness regulates degradation of MST2 via SCF βTrCP.
527 Biochimica et Biophysica Acta (BBA) - General Subjects 1866, 130238.
528 https://doi.org/10.1016/j.bbagen.2022.130238
529 Fulford, A.D., Holder, M.V., Frith, D., Snijders, A.P., Tapon, N., Ribeiro, P.S., 2019. Casein
530 kinase 1 family proteins promote Slimb-dependent Expanded degradation. eLife 8,
531 e46592. https://doi.org/10.7554/eLife.46592
532 Genevet, A., Wehr, M.C., Brain, R., Thompson, B.J., Tapon, N., 2010. Kibra Is a Regulator of the
533 Salvador/Warts/Hippo Signaling Network. Developmental Cell 18, 300–308.
534 https://doi.org/10.1016/j.devcel.2009.12.011
535 Guilak, F., Erickson, G.R., Ting-Beall, H.P., 2002. The Effects of Osmotic Stress on the
536 Viscoelastic and Physical Properties of Articular Chondrocytes. Biophysical Journal 82,
537 720–727. https://doi.org/10.1016/S0006-3495(02)75434-9
538 Hamaratoglu, F., Willecke, M., Kango-Singh, M., Nolo, R., Hyun, E., Tao, C., Jafar-Nejad, H.,
539 Halder, G., 2006. The tumour-suppressor genes NF2/Merlin and Expanded act through
540 Hippo signalling to regulate cell proliferation and apoptosis. Nature Cell Biology 8, 27–
541 36. https://doi.org/10.1038/ncb1339
542 Hannaford, M., Loyer, N., Tonelli, F., Zoltner, M., Januschke, J., 2019a. A chemical-genetics
543 approach to study the role of atypical protein kinase C in *Drosophila*. Development
544 dev.170589. https://doi.org/10.1242/dev.170589
545 Hannaford, M., Loyer, N., Tonelli, F., Zoltner, M., Januschke, J., 2019b. A chemical-genetics
546 approach to study the role of atypical protein kinase C in *Drosophila*. Development
547 dev.170589. https://doi.org/10.1242/dev.170589
548 Hariharan, I.K., 2015. Organ Size Control: Lessons from Drosophila. Developmental Cell 34,
549 255–265. https://doi.org/10.1016/j.devcel.2015.07.012
550 Huang, H.-L., Wang, S., Yin, M.-X., Dong, L., Wang, C., Wu, W., Lu, Y., Feng, M., Dai, C., Guo,
551 X., Li, L., Zhao, B., Zhou, Z., Ji, H., Jiang, J., Zhao, Y., Liu, X.-Y., Zhang, L., 2013. Par-
552 1 Regulates Tissue Growth by Influencing Hippo Phosphorylation Status and Hippo-
553 Salvador Association. PLoS Biology 11, e1001620.
554 https://doi.org/10.1371/journal.pbio.1001620
555 Ibar, C., Kirichenko, E., Keepers, B., Enners, E., Fleisch, K., Irvine, K.D., 2018. Tension-
556 dependent regulation of mammalian Hippo signaling through LIMD1. J Cell Sci 131,
557 jcs214700. https://doi.org/10.1242/jcs.214700
558 Lecuit, T., Lenne, P.-F., Munro, E., 2011. Force Generation, Transmission, and Integration during
559 Cell and Tissue Morphogenesis. Annu. Rev. Cell Dev. Biol. 27, 157–184.
560 https://doi.org/10.1146/annurev-cellbio-100109-104027
561 Lee, S., Wang, J.-W., Yu, W., Lu, B., 2012. Phospho-dependent ubiquitination and degradation of
562 PAR-1 regulates synaptic morphology and tau-mediated Aβ toxicity in Drosophila. Nat
563 Commun 3, 1312. https://doi.org/10.1038/ncomms2278
564 LeGoff, L., Rouault, H., Lecuit, T., 2013. A global pattern of mechanical stress polarizes cell
565 divisions and cell shape in the growing *Drosophila* wing disc. Development 140, 4051–
566 4059. https://doi.org/10.1242/dev.090878

López-Gay, J.M., Nunley, H., Spencer, M., di Pietro, F., Guirao, B., Bosveld, F., Markova, O., Gaugue, I., Pelletier, S., Lubensky, D.K., Bellaïche, Y., 2020. Apical stress fibers enable a scaling between cell mechanical response and area in epithelial tissue. Science 370, eabb2169. https://doi.org/10.1126/science.abb2169

Ma, X., Guo, X., Richardson, H.E., Xu, T., Xue, L., 2018. POSH regulates Hippo signaling through ubiquitin-mediated expanded degradation. Proceedings of the National Academy of Sciences 201715165. https://doi.org/10.1073/pnas.1715165115

Mao, Y., Tournier, A.L., Hoppe, A., Kester, L., Thompson, B.J., Tapon, N., 2013. Differential proliferation rates generate patterns of mechanical tension that orient tissue growth. EMBO J 32, 2790–2803. https://doi.org/10.1038/emboj.2013.197

Misra, J.R., Irvine, K.D., 2019. Early girl is a novel component of the Fat signaling pathway. PLoS Genet 15, e1007955. https://doi.org/10.1371/journal.pgen.1007955

Morais-de-Sá, E., Vega-Rioja, A., Trovisco, V., St Johnston, D., 2013. Oskar Is Targeted for Degradation by the Sequential Action of Par-1, GSK-3, and the SCF-Slimb Ubiquitin Ligase. Developmental Cell 26, 303–314. https://doi.org/10.1016/j.devcel.2013.06.011

Pan, Y., Heemskerk, I., Ibar, C., Shraiman, B.I., Irvine, K.D., 2016. Differential growth triggers mechanical feedback that elevates Hippo signaling. Proceedings of the National Academy of Sciences 113, E6974–E6983. https://doi.org/oskar

Piekny, A., Werner, M., Glotzer, M., 2005. Cytokinesis: welcome to the Rho zone. Trends in Cell Biology 15, 651–658. https://doi.org/10.1016/j.tcb.2005.10.006

Pietuch, A., Brückner, B.R., Janshoff, A., 2013. Membrane tension homeostasis of epithelial cells through surface area regulation in response to osmotic stress. Biochimica et Biophysica Acta (BBA) - Molecular Cell Research 1833, 712–722. https://doi.org/10.1016/j.bbamcr.2012.11.006

Pinheiro, D., Hannezo, E., Herszterg, S., Bosveld, F., Gaugue, I., Balakireva, M., Wang, Z., Cristo, I., Rigaud, S.U., Markova, O., Bellaïche, Y., 2017. Transmission of cytokinesis forces via E-cadherin dilution and actomyosin flows. Nature 545, 103–107. https://doi.org/10.1038/nature22041

Rauskolb, C., Cervantes, E., Madere, F., Irvine, K.D., 2019. Organization and function of tension-dependent complexes at adherens junctions. Journal of Cell Science 132, jcs224063. https://doi.org/10.1242/jcs.224063

Rauskolb, C., Sun, S., Sun, G., Pan, Y., Irvine, K.D., 2014. Cytoskeletal Tension Inhibits Hippo Signaling through an Ajuba-Warts Complex. Cell 158, 143–156. https://doi.org/10.1016/j.cell.2014.05.035

Ribeiro, P., Holder, M., Frith, D., Snijders, A.P., Tapon, N., 2014. Crumbs promotes expanded recognition and degradation by the SCFSlimb/ -TrCP ubiquitin ligase. Proceedings of the National Academy of Sciences 111, E1980–E1989. https://doi.org/10.1073/pnas.1315508111

Rodrigues-Campos, M., Thompson, B.J., 2014. The ubiquitin ligase FbxL7 regulates the Dachsous-Fat-Dachs system in Drosophila. Development 141, 4098–4103. https://doi.org/10.1242/dev.113498

Roffay, C., Molinard, G., Kim, K., Urbanska, M., Andrade, V., Barbarasa, V., Nowak, P., Mercier, V., García-Calvo, J., Matile, S., Loewith, R., Echard, A., Guck, J., Lenz, M., Roux, A., 2021. Passive coupling of membrane tension and cell volume during active response of cells to osmosis. Proc Natl Acad Sci USA 118, e2103228118. https://doi.org/10.1073/pnas.2103228118

613 Sansores-Garcia, L., Bossuyt, W., Wada, K.-I., Yonemura, S., Tao, C., Sasaki, H., Halder, G.,
614 2011. Modulating F-actin organization induces organ growth by affecting the Hippo
615 pathway. The EMBO journal 30, 2325–2335.
616 Sarpal, R., Yan, V., Kazakova, L., Sheppard, L., Yu, J.C., Fernandez-Gonzalez, R., Tepass, U.,
617 2019. Role of α-Catenin and its mechanosensing properties in regulating Hippo/YAP-
618 dependent tissue growth. PLoS Genet 15, e1008454.
619 https://doi.org/10.1371/journal.pgen.1008454
620 Sinha, B., Köster, D., Ruez, R., Gonnord, P., Bastiani, M., Abankwa, D., Stan, R.V., Butler-
621 Browne, G., Vedie, B., Johannes, L., Morone, N., Parton, R.G., Raposo, G., Sens, P.,
622 Lamaze, C., Nassoy, P., 2011. Cells Respond to Mechanical Stress by Rapid Disassembly
623 of Caveolae. Cell 144, 402–413. https://doi.org/10.1016/j.cell.2010.12.031
624 Stewart, M.P., Helenius, J., Toyoda, Y., Ramanathan, S.P., Muller, D.J., Hyman, A.A., 2011.
625 Hydrostatic pressure and the actomyosin cortex drive mitotic cell rounding. Nature 469,
626 226–230. https://doi.org/10.1038/nature09642
627 Stringer, C., Wang, T., Michaelos, M., Pachitariu, M., 2021. Cellpose: a generalist algorithm for
628 cellular segmentation. Nat Methods 18, 100–106. https://doi.org/10.1038/s41592-020-
629 01018-x
630 Su, T., Ludwig, M.Z., Xu, J., Fehon, R.G., 2017. Kibra and Merlin Activate the Hippo Pathway
631 Spatially Distinct from and Independent of Expanded. Developmental Cell 40, 478-
632 490.e3. https://doi.org/10.1016/j.devcel.2017.02.004
633 Tokamov, S.A., Su, T., Ullyot, A., Fehon, R.G., 2021. Negative feedback couples Hippo pathway
634 activation with Kibra degradation independent of Yorkie-mediated transcription. eLife 10,
635 e62326. https://doi.org/10.7554/eLife.62326
636 Uehata, M., Ishizaki, T., Satoh, H., Ono, T., Kawahara, T., Morishita, T., Tamakawa, H.,
637 Yamagami, K., Inui, J., Maekawa, M., Narumiya, S., 1997. Calcium sensitization of
638 smooth muscle mediated by a Rho-associated protein kinase in hypertension. Nature 389,
639 990–994. https://doi.org/10.1038/40187
640 van der Walt, S., Schönberger, J.L., Nunez-Iglesias, J., Boulogne, F., Warner, J.D., Yager, N.,
641 Gouillart, E., Yu, T., 2014. scikit-image: image processing in Python. PeerJ 2, e453.
642 https://doi.org/10.7717/peerj.453
643 Wada, K.-I., Itoga, K., Okano, T., Yonemura, S., Sasaki, H., 2011. Hippo pathway regulation by
644 cell morphology and stress fibers. Development 138, 3907–3914.
645 https://doi.org/10.1242/dev.070987
646 Wang, X., Zhang, Y., Blair, S.S., 2019. Fat-regulated adaptor protein Dlish binds the growth
647 suppressor Expanded and controls its stability and ubiquitination. Proceedings of the
648 National Academy of Sciences 116, 1319–1324. https://doi.org/10.1073/pnas.1811891116
649 Williams, A.M., Donoughe, S., Munro, E., Horne-Badovinac, S., 2022. Fat2 polarizes the WAVE
650 complex in trans to align cell protrusions for collective migration. eLife 11, e78343.
651 https://doi.org/10.7554/eLife.78343
652 Xu, J., Su, T., Tokamov, S.A., Fehon, R.G., 2019. Live Imaging of Hippo Pathway Components
653 in Drosophila Imaginal Discs, in: Hergovich, A. (Ed.), The Hippo Pathway, Methods in
654 Molecular Biology. Springer New York, New York, NY, pp. 53–59.
655 https://doi.org/10.1007/978-1-4939-8910-2_4
656 Xu, J., Vanderzalm, P.J., Ludwig, M., Su, T., Tokamov, S.A., Fehon, R.G., 2018. Yorkie
657 Functions at the Cell Cortex to Promote Myosin Activation in a Non-transcriptional

658 Manner. Developmental Cell 46, 271-284.e5.
659 https://doi.org/10.1016/j.devcel.2018.06.017
660 Yee, W.B., Delaney, P.M., Vanderzalm, P.J., Ramachandran, S., Fehon, R.G., 2019. The CAF-1
661 complex couples Hippo pathway target gene expression and DNA replication. MBoC 30,
662 2929–2942. https://doi.org/10.1091/mbc.E19-07-0387
663 Yu, J., Zheng, Y., Dong, J., Klusza, S., Deng, W.-M., Pan, D., 2010a. Kibra Functions as a Tumor
664 Suppressor Protein that Regulates Hippo Signaling in Conjunction with Merlin and
665 Expanded. Developmental Cell 18, 288–299.
666 https://doi.org/10.1016/j.devcel.2009.12.012
667 Yu, J., Zheng, Y., Dong, J., Klusza, S., Deng, W.-M., Pan, D., 2010b. Kibra Functions as a Tumor
668 Suppressor Protein that Regulates Hippo Signaling in Conjunction with Merlin and
669 Expanded. Developmental Cell 18, 288–299.
670 https://doi.org/10.1016/j.devcel.2009.12.012
671 Zhang, L., Ward, R.E., 2011. Distinct tissue distributions and subcellular localizations of
672 differently phosphorylated forms of the myosin regulatory light chain in Drosophila.
673 Gene Expression Patterns 11, 93–104. https://doi.org/10.1016/j.gep.2010.09.008

Figure 1

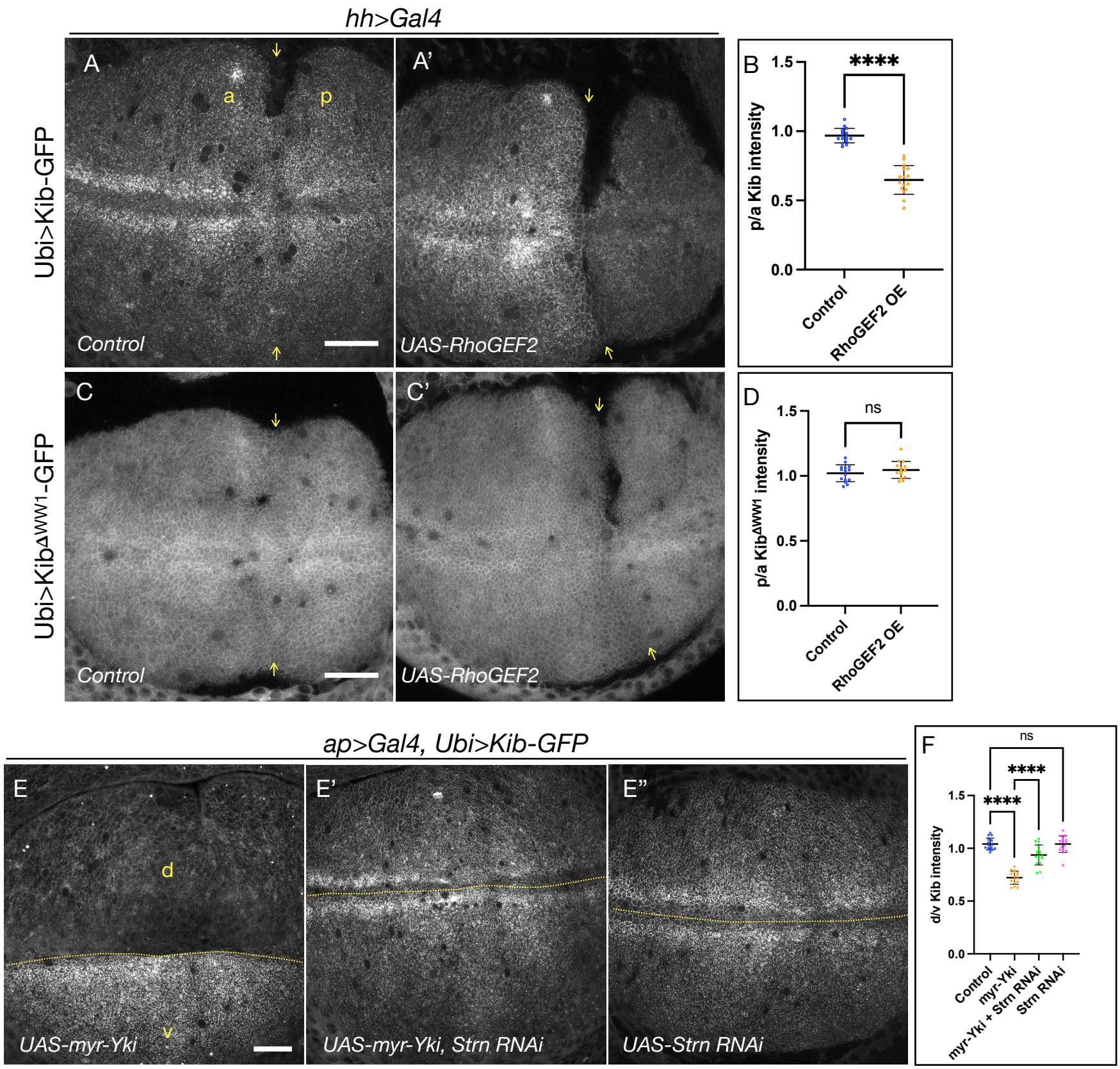
hh>Gal4
Ubi>Kib-GFP
A
a
p
Control
A'
UAS-RhoGEF2
B
****
p/a Kib intensity
1.5
1.0
0.5
0.0
Control
RhoGEF2 OE
Ubi>KibΔWW1-GFP
C
Control
C'
UAS-RhoGEF2
D
ns
p/a KibΔWW1 intensity
1.5
1.0
0.5
0.0
Control
RhoGEF2 OE
ap>Gal4, Ubi>Kib-GFP
E
d
v
UAS-myr-Yki
E'
UAS-myr-Yki, Strn RNAi
E''
UAS-Strn RNAi
F
ns
****
****
d/v Kib intensity
1.5
1.0
0.5
0.0
Control
myr-Yki
myr-Yki + Strn RNAi
Strn RNAi

Figure 1: Cortical tension promotes Kib degradation.
A-A') Compared to control tissues (A), ectopic RhoGEF2 expression results in a significant decrease in Kib abundance (A'). Yellow arrows indicate anterior-posterior (a-p) boundary.
B) Plot of p/a ratio of Ubi>Kib-GFP mean fluorescence intensity under the conditions shown in A-A'.
C-C') In contrast to wild-type Kib, Kib$^{\Delta WW1}$ is not affected by RhoGEF2 expression.
D) Plot of p/a ratio of Ubi>Kib$^{\Delta WW1}$-GFP mean fluorescence intensity under the conditions shown in C-C'.
E-E'') Ectopic myr-Yki expression leads to a significant decrease in Kib abundance (E), and depletion of Strn-MLCK suppresses the effect of myr-Yki expression (E'). Depletion of Strn-MLCK alone has no effect on Kib abundance (E''). Dashed lines indicate the dorsal-ventral (d-v) boundary. Scale bars = 20μm.
F) Plot of d/v ratio of Ubi>Kib-GFP mean fluorescence intensity under the conditions shown in E-E'' (a representative control image of Ubi>Kib-GFP is shown in A).
Unless indicated otherwise, statistical significance for two group comparisons was calculated using Mann-Whitney test. For more than two groups, One-way ANOVA followed by Tukey's HSD test was used. Also, unless otherwise noted data are shown as the mean ± SD and significance values are represented as follows: ****$p \leq 0.0001$, ***$p \leq 0.0001$, **$p \leq 0.001$, *$p \leq 0.05$, ns = not significant.

Figure 2

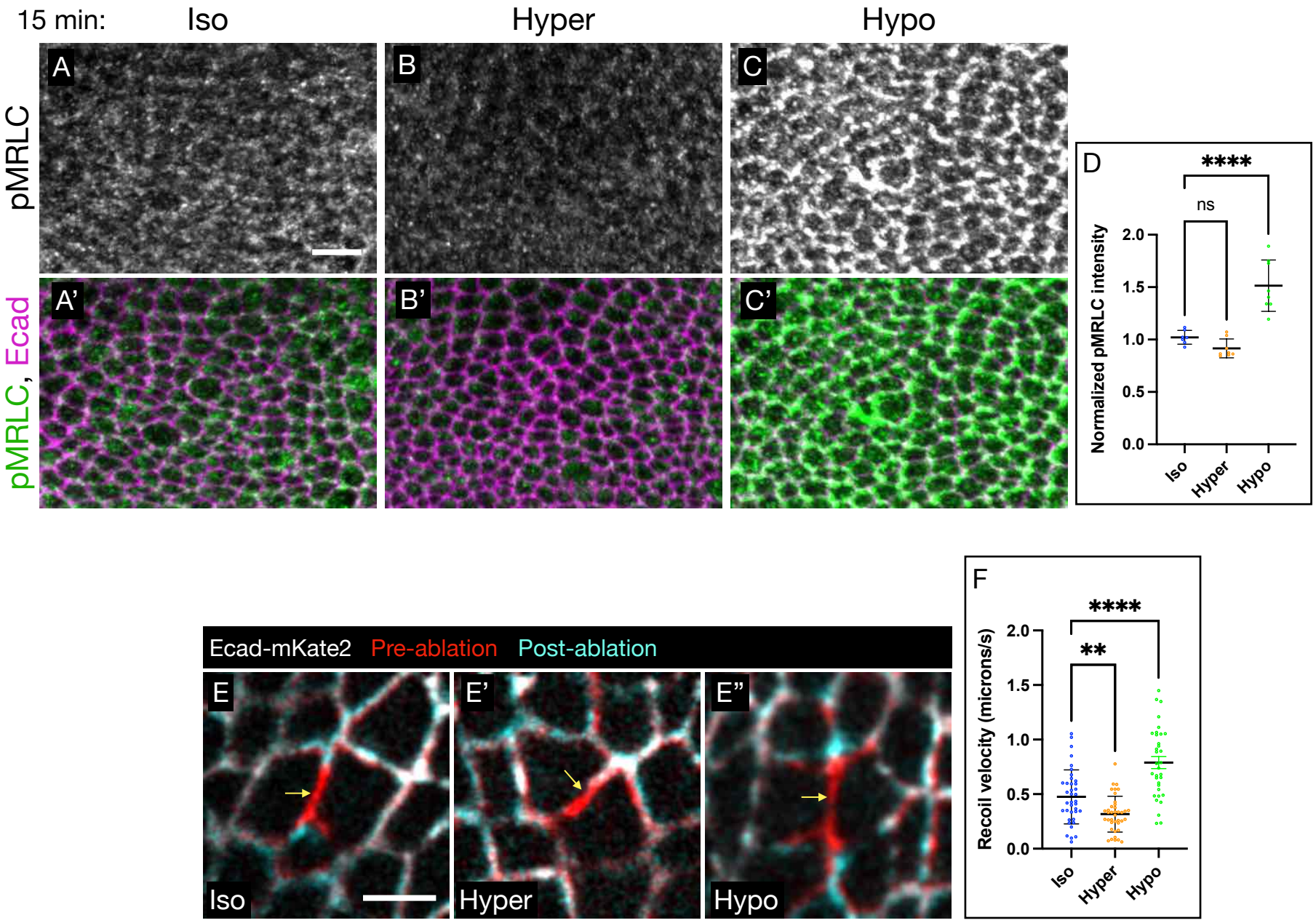
15 min:
Iso
Hyper
Hypo
pMRLC
pMRLC, Ecad
A
B
C
A'
B'
C'
D
****
ns
Normalized pMRLC intensity
2.0
1.5
1.0
0.5
0.0
Iso
Hyper
Hypo
Ecad-mKate2
Pre-ablation
Post-ablation
E
E'
E"
Iso
Hyper
Hypo
F
****
**
Recoil velocity (microns/s)
2.0
1.5
1.0
0.5
0.0
Iso
Hyper
Hypo

Figure 2: Changes in osmotic conditions alter myosin activity and cortical tension.
A-C) Compared to isotonic conditions (A-A'), hypertonic conditions lead to a slight decrease in pMRLC (B-B'), whereas hypotonic conditions significantly increase pMRLC signal (C-C'). Scale bar = 5μm.
D) Quantification of mean pMRLC intensity under osmotic conditions shown in A-C.
E-E'') Representative overlay images of Ecad-mKate2 in wing imaginal disc cells pre- (red) and post-ablation of bicellular junctions (arrows) under isotonic (E), hypertonic (E'), hypotonic E'') conditions. Scale bar = 3μm.
F) Quantification of initial junction recoil velocities measured from the ablation experiments.

Figure 3

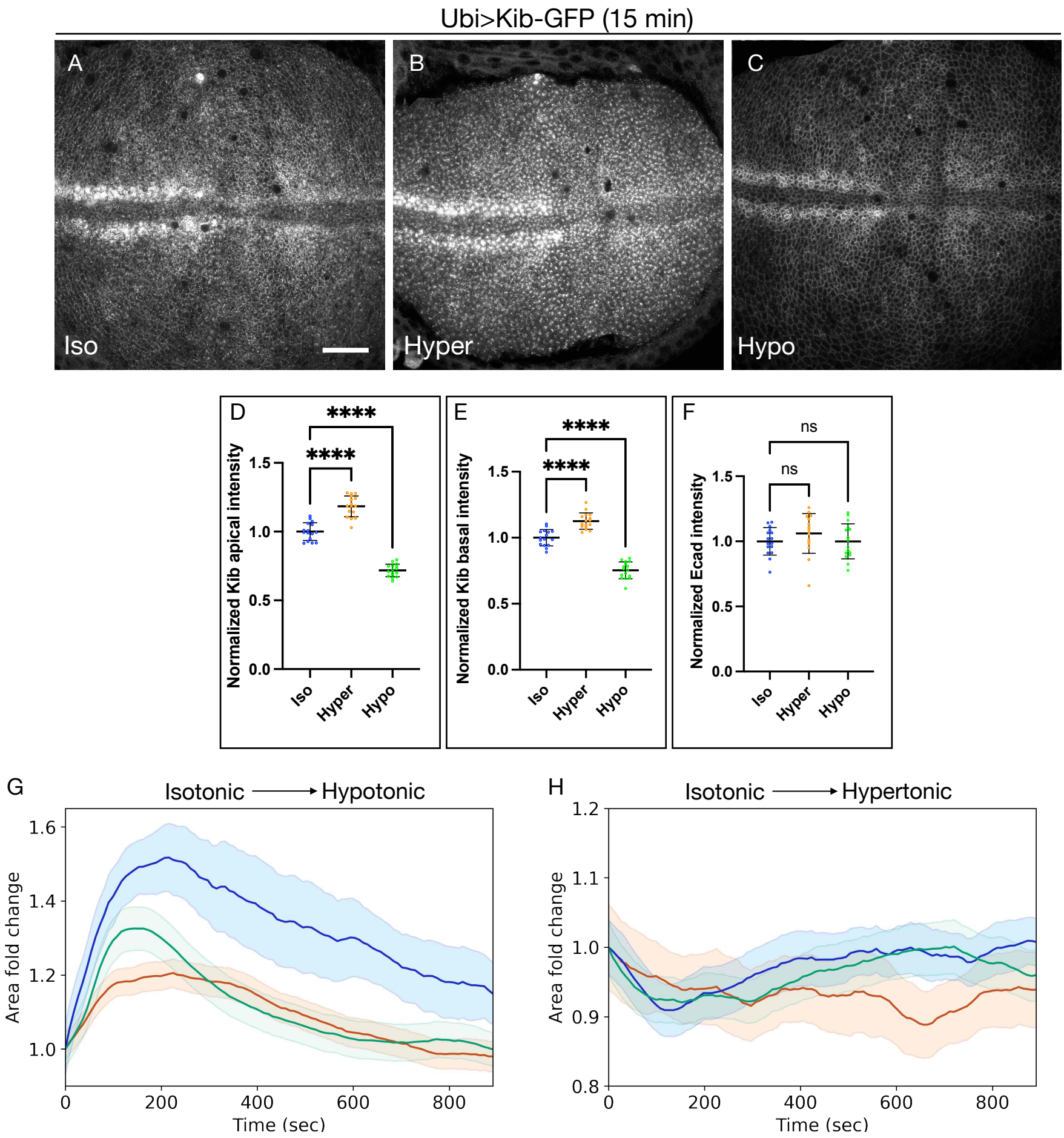
Ubi>Kib-GFP (15 min)
A
Iso
B
Hyper
C
Hypo
D
****
****
Normalized Kib apical intensity
1.5
1.0
0.5
0.0
Iso
Hyper
Hypo
E
****
****
Normalized Kib basal intensity
1.5
1.0
0.5
0.0
Iso
Hyper
Hypo
F
ns
ns
Normalized Ecad intensity
1.5
1.0
0.5
0.0
Iso
Hyper
Hypo
G
Isotonic → Hypotonic
Area fold change
1.6
1.4
1.2
1.0
0
200
400
600
800
Time (sec)
H
Isotonic → Hypertonic
Area fold change
1.2
1.1
1.0
0.9
0.8
0
200
400
600
800
Time (sec)

Figure 3: Osmotic shifts affect Kib abundance.
A-C) Compared to isotonic conditions (A), hypertonic shift results in higher Kib abundance (B), while hypotonic shift leads to decreased Kib abundance (C). Scale bar = 20μm.
D-F') Quantification of apical Kib-GFP (D), basal Kib-GFP (E), and apical Ecad-mKate2 (F) mean fluorescence.
G & H) Plots of cell area changes (mean ± SEM) obtained from tissues shifted from isotonic to hypotonic (G) or isotonic to hypertonic (H) conditions. Each curve represents an independent trial/tissue, with three tissues imaged for each condition.

Figure 4

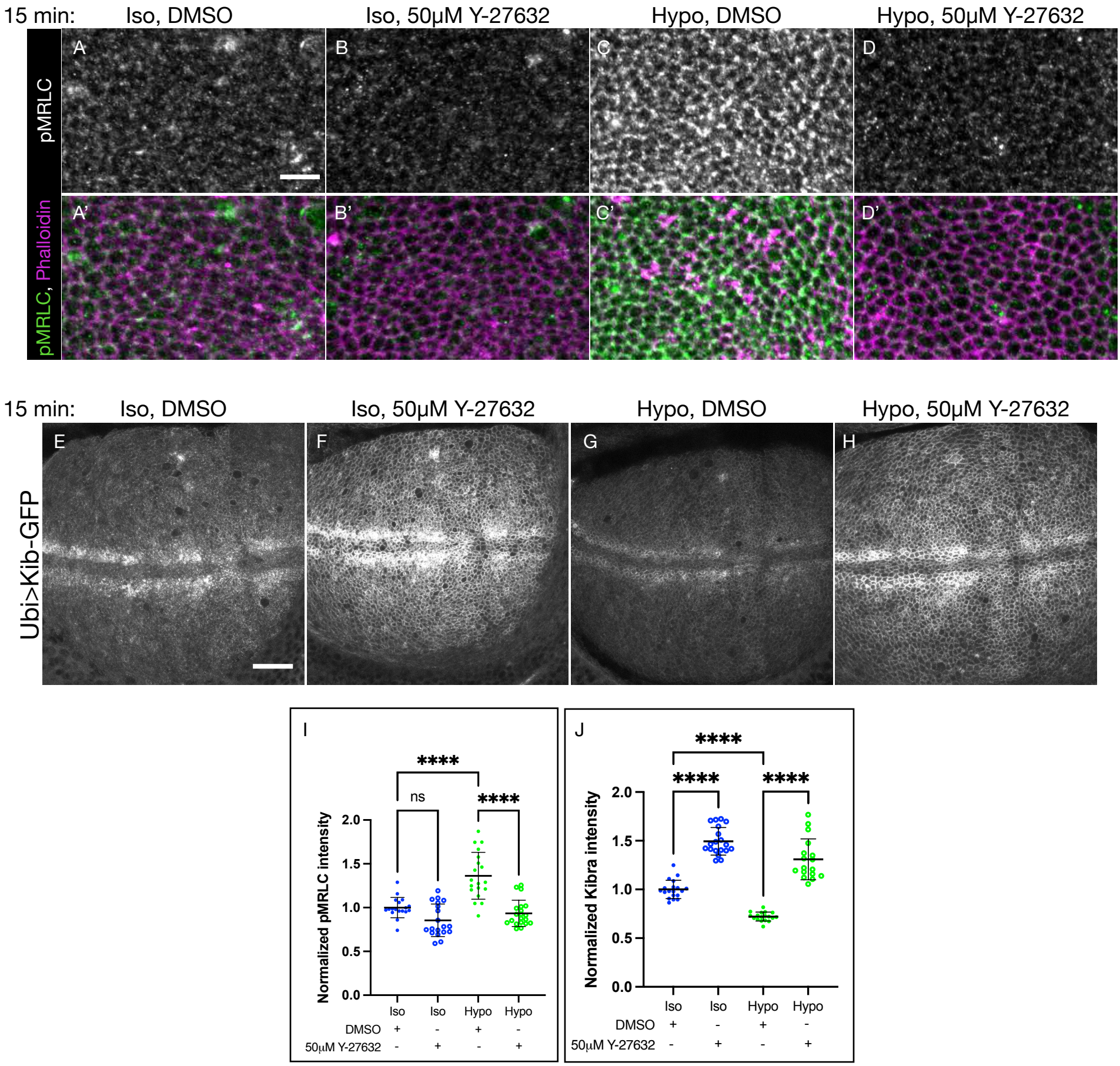
15 min:
Iso, DMSO
Iso, 50μM Y-27632
Hypo, DMSO
Hypo, 50μM Y-27632
pMRLC
pMRLC, Phalloidin
A
B
C
D
A'
B'
C'
D'
15 min:
Iso, DMSO
Iso, 50μM Y-27632
Hypo, DMSO
Hypo, 50μM Y-27632
Ubi>Kib-GFP
E
F
G
H
I
Normalized pMRLC intensity
2.0
1.5
1.0
0.5
0.0
****
ns
****
Iso
Iso
Hypo
Hypo
DMSO + - + -
50μM Y-27632 - + - +
J
Normalized Kibra intensity
2.0
1.5
1.0
0.5
0.0
****
****
****
Iso
Iso
Hypo
Hypo
DMSO + - + -
50μM Y-27632 - + - +

Figure 4: Treatment with Y-27632 raises Kib abundance and reverses the effect of hypotonic shift.

A-D') Staining with the antibody against pMRLC shows that Y-27632 treatment leads to a slight decrease in pMRLC staining under isotonic conditions (A-B') and a blocks pMRLC upregulation under hypotonic shift (C-D'). Scale bar = 5µm.

E-H) Compared to control (E), treatment with Y-27632 dramatically increases Kib abundance under isotonic conditions (F). Addition of Y-27632 also blocks the decrease in Kib abundance induced by hypotonic shift (G & H). Scale bar = 20µm.

I) Plot of normalized mean pMRLC intensities obtained from experiments represented in A-D'.

J) Plot of normalized mean Kib-GFP intensities obtained from experiments represented in E-H.

Figure 5

IP:HA

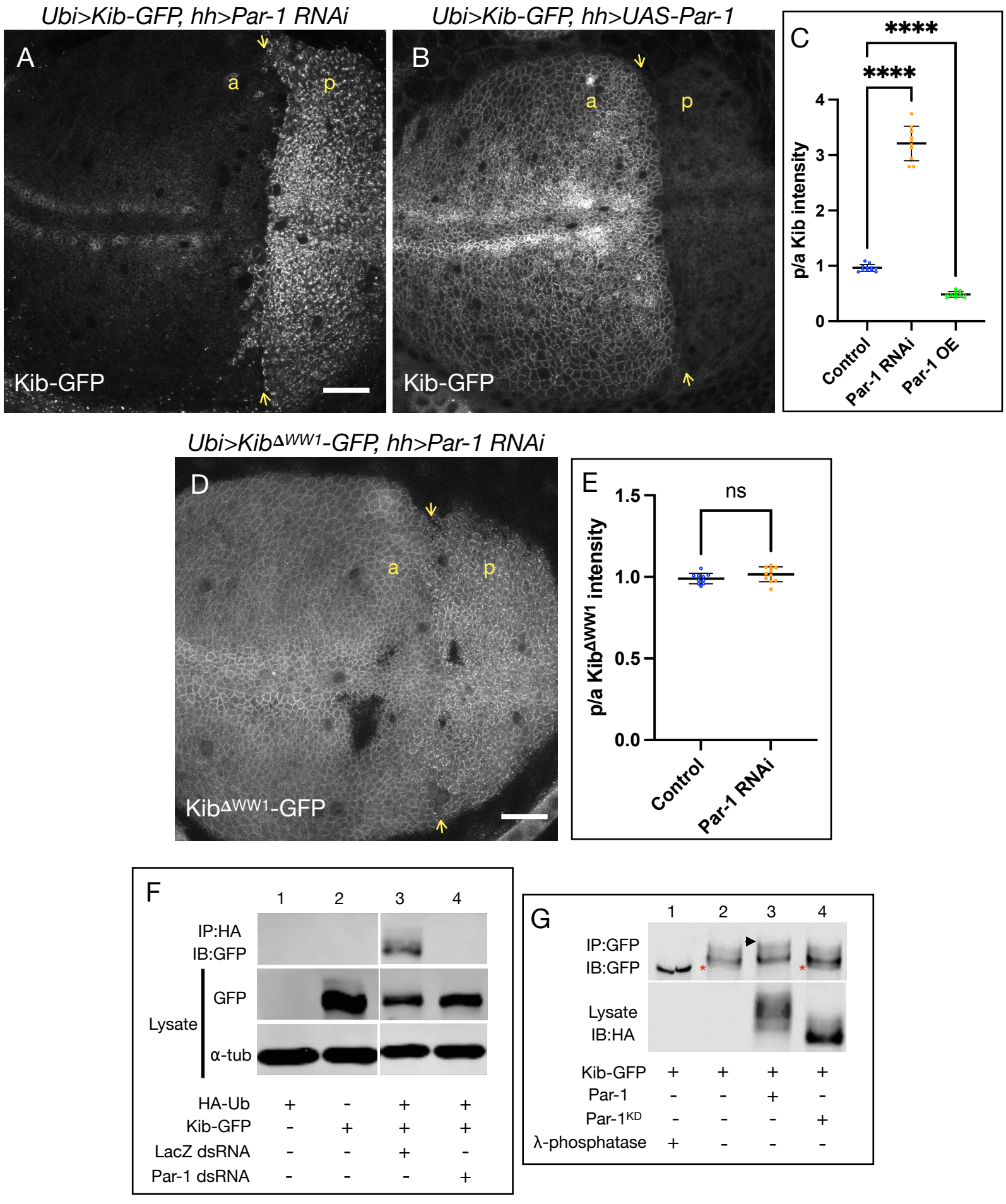

Figure 5. Par-1 promotes ubiquitin-mediated Kib degradation.
A) Loss of Par-1 in the posterior wing disc compartment leads to a dramatic increase in Kib abundance. Yellow arrows indicate the anterior-posterior (a-p) boundary. Scale bar = 20μm.
B) Ectopic Par-1 expression in the posterior wing disc compartment results in a strong decrease Kib abundance.
C) Quantification of loss or gain of Par-1 function on Kib abundance as a posterior/anterior (p/a) ratio of mean fluorescence intensity.
D) Loss of Par-1 in the posterior wing disc compartment does not affect $Kib^{\Delta WW1}$ abundance.
E) Quantification of the effect of Par-1 depletion on $Kib^{\Delta WW1}$ abundance as a p/a ratio of mean fluorescence intensity.
F) Kib immunoprecipitated from cultured S2 cells is normally ubiquitinated when cells are treated with a control LacZ dsRNA (lane 3). Depletion of Par-1 with dsRNA results in decreased Kib ubiquitination (lane 4).
G) Treatment of Kib samples immunoprecipitated from S2 cells with λ-phosphatase results in non-phosphorylated, faster migrating band (lane 1) relative to phosphorylated, slower migrating bands observed without λ-phosphatase treatment (lane 2). Expression of wild-type Par-1, but not kinase-dead Par-1, leads to increased Kib phosphorylation (lanes 3 & 4). Asterisks indicate non-phosphorylated Kib pool, which disappears upon Par-1 expression. Arrowhead indicates a slower migrating (more phosphorylated) Kib pool.

Figure 6

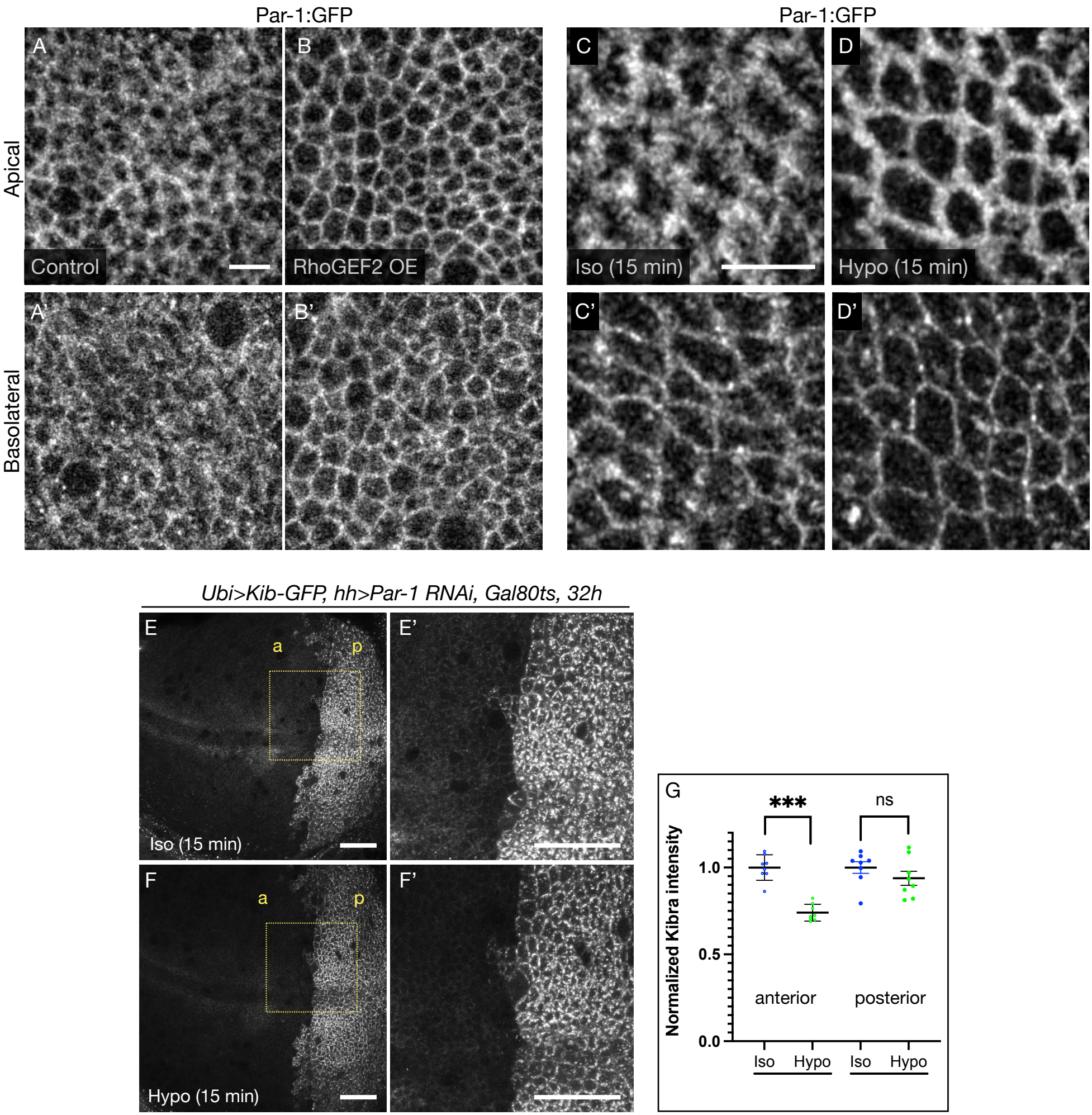
Par-1:GFP
Par-1:GFP
Apical
Basolateral
A
B
C
D
A'
B'
C'
D'
Control
RhoGEF2 OE
Iso (15 min)
Hypo (15 min)
Ubi>Kib-GFP, hh>Par-1 RNAi, Gal80ts, 32h
E
E'
F
F'
a
p
Iso (15 min)
Hypo (15 min)
G
***
ns
Normalized Kibra intensity
1.0
0.5
0.0
anterior
posterior
Iso
Hypo
Iso
Hypo

Figure 6: Cortical tension regulates Kib abundance by modulating cortical Par-1 association.

A & B') Compared to control cells (A-A'), ectopic RhoGEF2 expression leads to tighter Par-1 association with the apical and basolateral cell cortex (B-B'). Scale bar = 5μm.

C & D') Compared to isotonic conditions (C-C'), Par-1 becomes more tightly associated with the apical and basolateral cell cortex upon hypotonic shift (D-D'). Scale bar = 5μm.

E-G) Under isotonic conditions, depletion of Par-1 in the posterior compartment (p) leads to a significant increase in Kib levels (E & E', G). Shift to hypotonic conditions leads to a significant decrease in Kib abundance in the anterior region, but only a mild (not statistically significant) decrease in the posterior region where Par-1 was depleted (F & F', G). Scale bars = 20μm.